ACS APPLIED MATERIALS & INTERFACES

Research Article

www.acsami.org

Optimizing Nonlinear Optical Visibility of Two-Dimensional Materials

Xianchong Miao,[†,§,⊥] Ningning Xuan,[‡,⊥] Qi Liu,[†,§] Weishu Wu,[†,§] Hanqi Liu,[‡] Zhengzong Sun,*[,‡] and Minbiao Ji*[,†,§]

[†]State Key Laboratory of Surface Physics and Department of Physics, Key Laboratory of Micro and Nano Photonic Structures (Ministry of Education), Collaborative Innovation Center of Genetics and Development, and [‡]Department of Chemistry and Shanghai Key Laboratory of Molecular Catalysis and Innovative Materials, Fudan University, Shanghai 200433, China

[§]Collaborative Innovation Center of Advanced Microstructure, Nanjing 210093, China

Supporting Information

ABSTRACT: Two-dimensional (2D) materials have attracted broad research interests across various nonlinear optical (NLO) studies, including nonlinear photoluminescence (NPL), second harmonic generation (SHG), transient absorption (TA), and so forth. These studies have unveiled important features and information of 2D materials, such as in grain boundaries, defects, and crystal orientations. However, as most research studies focused on the intrinsic NLO processes, little attention has been paid to the substrates underneath. Here, we discovered that the NLO signal depends significantly on the thickness of SiO_2 in SiO_2/Si substrates. A 40-fold enhancement of the NPL signal of graphene was observed when the SiO_2 thickness was varied from 270 to 125 nm under 800 nm excitation. We systematically studied the NPL intensity of graphene on three different SiO_2 thicknesses within a pump wavelength range of 800−1100 nm. The results agreed with a numerical model based on back reflection and interference. Furthermore, we have extended our measurements to include TA and SHG of graphene and MoS_2, confirming that SiO_2 thickness has similar effects on all of the three major types of NLO signals. Our results will serve as an important guidance for choosing the optimum substrates to conduct NLO research studies on 2D materials.

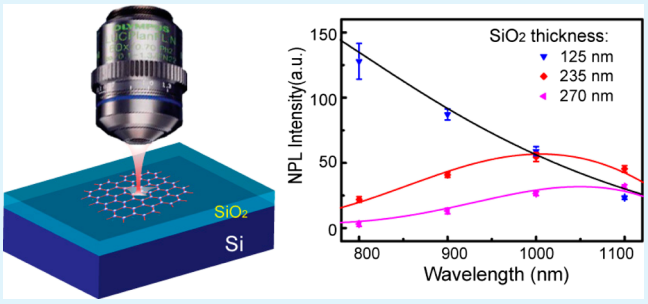

KEYWORDS: *nonlinear optics, two-dimensional materials, nonlinear optical microscopy, transient absorption, nonlinear photoluminescence, SiO_2 thickness*

1. INTRODUCTION

Two-dimensional (2D) materials have drawn enormous research attentions owing to their unique electrical, optical, and chemical properties. For instance, the "Dirac cone" band structure of graphene results in its high mobility, quantum Hall effect, and Klein tunneling effect;[1] the valley structure of transition metal dichalcogenide (TMDC) has boosted the research studies of "valleytronics";[2] and the more recent black phosphorus (BP) has unique electronic property and strong anisotropy.[3,4] As a result, these 2D materials have shown excellent device performances such as in field-effect transistors, integrated circuits, solar cells, and light-emitting diodes.[5−8] Furthermore, various van der Waals heterostructures can be constructed with these 2D materials, where the interactions between them could influence their electronic and optoelectronic properties,[9] leading to a rapidly growing research area.[10−12]

Although atomically thin, many 2D materials have demonstrated exotic optical responses. In linear optics, the universal absorbance ($e^2/4\hbar$) of single-layer graphene is well-known;[13] TMDCs such as single-layered MoS_2 have shown strong and valley-selective photoluminescence (PL);[14,15] and BP has demonstrated layer-dependent exciton emissions.[16−18]

In nonlinear optics, a rapidly growing interest has been focused on various nonlinear optical (NLO) properties of 2D materials, which are usually orders of magnitude stronger than conventional bulk materials.[19−21] These NLO processes could be divided into three major categories. First, coherent optical parametric processes, such as second harmonic generation (SHG),[22] third harmonic generation (THG), and four-wave mixing (FWM).[23,24] For instance, graphene generates strong THG and FWM signals, whereas MoS_2 has unique SHG property that reflects its crystal symmetry in mono- and few-layered samples. Second, nonlinear dissipative processes, including transient absorption (TA), two-photon absorption (TPA), and saturable absorption, that pump electrons into an excited state.[25−29] In particular, TA could be used to learn the transient dynamics of excited photocarriers through a pump-probe-based method and reveal ultrafast electron−electron or electron−phonon interactions. Third, incoherent photon up-conversion processes, such as two-photon fluorescence of MoS_2 and nonlinear PL (NPL) of graphene.[30−32] All of these NLO

Received: July 7, 2017
Accepted: September 14, 2017
Published: September 14, 2017

DOI: 10.1021/acsami.7b09807
ACS Appl. Mater. Interfaces 2017, 9, 34448−34455

properties of 2D materials have been explored and utilized in optical microscopy, both for material and biological sciences.[33−36]

Despite extensive studies, the relationship between the NLO intensity of 2D materials and the thickness of their substrates has never been seriously investigated, whereas the thickness-dependent linear optical contrast of graphene has been well-studied and applied to optimize its visibility.[37,38] In fact, the choice of SiO_2/Si substrates used for the NLO measurements appears quite random throughout the literature studies. Three major commercially available thicknesses of SiO_2 have been used: 90, 200, and 285 nm, even for measuring the same 2D material.[3,39−42] Besides, large discrepancies exist among experiments measuring the same NLO susceptibility of graphene with the same SiO_2 thickness but different excitation wavelengths.[23,43,44] Therefore, it is worth quantifying the relationship between the NLO intensities of 2D materials and the underneath SiO_2 thickness. Here, we carefully measured the NPL intensities of graphene as functions of the SiO_2 thickness and excitation wavelength, the results of which were explained by our numerical model based on the interference of the excitation laser. The interference between the forward and back-reflected beams creates partial standing waves that have varying intensity profiles in the sample planes, depending on the SiO_2 thickness. We chose NPL because it is dominated by the incoherent process that requires only one excitation beam and thus simplifies the modeling. More than 1 order of magnitude difference could be seen between different SiO_2 thicknesses, proving the crucial role of such an effect in NLO signal generation, which was underestimated previously. Furthermore, we have extended our measurements to include the other two major types of NLO processes—TA of graphene and SHG of MoS_2. Compared with linear optics and NPL, additional factors need to be taken into account, such as the coherence of SHG emission and the interaction between pump and probe beams in TA measurements. Our simplified model could qualitatively agree with all of the above experimental results and may aid future NLO research studies of 2D materials.

2. EXPERIMENTAL SECTION

2.1. Optical Apparatus. We constructed a multimodality NLO microscopy system to measure the three types of NLO signals on synthesized graphene and MoS_2. The optical setup of the microscope system is shown in Figure 1, similar to the ones reported previously.[34,36,45] Two laser beams from a femtosecond optical parametric oscillator (OPO, InSight DS+, Newport, CA) were used as the light source for our NLO microscope. For NPL or SHG measurements, the tunable OPO output (800−1100 nm) was used to excite the samples, and the emission photons were collected through the same microscope objective, filtered by proper optical filters and detected with a photomultiplier tube (PMT). We used a short-pass filter (FF01-750SP, Semrock) for NPL measures and a narrow band-pass filter (FF01-405/10, Semrock) for SHG detection with 810 nm excitation. For TA measurements, a pump-probe-based optical setup was built, in which the fundamental 1040 nm beam was used as the pump, and the OPO output as the probe. Both beams were overlapped spatially and temporally, sent into the laser-scanning microscope (FV1200, Olympus), and focused onto the samples. To efficiently collect the back-reflected probe beam, a polarizing beam splitter (PBS) and a quarter wave plate were inserted before the objective lens. The intensity of the pump beam was modulated at 20 MHz by an electro-optical modulator (EOM). The probe beam was optically filtered, collected by a photodiode (PD), and demodulated with a commercial lock-in amplifier (HF2LI, Zurich Instruments) to extract the TA signals. All of the NLO signals were connected to the microscope inputs to form images. The 2D materials on different substrates were imaged with an air objective [UPLSAPO 20X, numerical aperture (NA) = 0.75, Olympus]. A cartoon illustration of light focusing onto 2D materials on top of the SiO_2/Si substrate is shown in Figure 1b. Laser powers at the samples were kept around 2 mW. Each 512 × 512 image was taken in ∼1 s, with 2 μs pixel dwell time. No detectable change of the NLO signal strength was observed during the measurements, indicating little sample degradation.

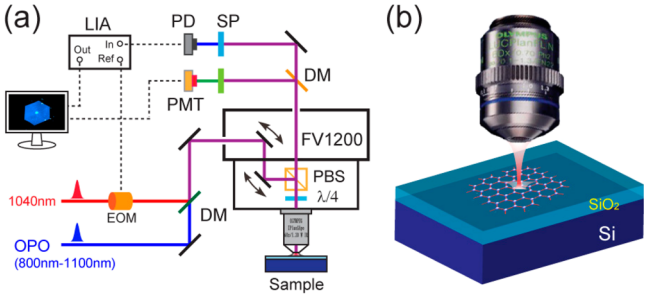

Figure 1. Schematics of the experimental design. (a) Optical setup of the NLO microscope. (b) Cartoon illustration of the focused laser beam onto the 2D materials on the Si/SiO_2 substrate. EOM: electro-optical modulator; LIA: lock-in amplifier; DM: dichroic mirror; PD: photodiode; PMT: photomultiplier tube; SP: short-pass optical filter; and PBS: polarizing beam splitter.

The three commercial SiO_2/Si substrates mentioned above were used to conduct the thickness-dependent NLO measurements, with the measured thicknesses of 125, 235, and 270 nm using an ellipsometer (UVISEL-2, Horiba). To clarify, we only analyzed the signal intensities of monolayer materials throughout the work, unless specifically stated.

2.2. Synthesis of Graphene. Single-crystal graphene synthesis and transfer processes are described as follows. A standard 1 in. quartz tube in a chemical vapor deposition (CVD) furnace was used as the reaction chamber. An electropolished 25 μm thick Cu foil (99.8%, Alfa Aesar) was used for growth. The cleaned Cu foil was annealed at 1050 °C for 1 h. Then, CH_4 (50 sccm of 1:99 CH_4/Ar mix) was added for a desired period of growth time. After the reaction, the samples were rapidly cooled to room temperature. Poly(methyl methacrylate) (43982PMMA, Alfa Aesar)-assisted method was used to transfer single-crystal graphene onto different substrates.

2.3. Synthesis of MoS_2. MoS_2 was synthesized in a standard 1 in. quartz tube and a two-zone CVD equipment to control the temperature of MoO_3 (99.9%, Aladdin) and S (99.5%, Sinopharm Chemical Reagent Co., Ltd.), respectively. MoO_3 (10 mg) and Te (30 mg, 99.999%, Sinopharm Chemical Reagent Co., Ltd.) powders were physically mixed and then placed in a ceramic boat at the center of the furnace. The Te powder was used to accelerate the volatilization of MoO_3 during growth.[46] The cleaned substrate with a different thickness of SiO_2 was placed facing down on the ceramic boat. Sulfur powder (>500 mg) was put at the center of another heating zone, which was about 20 cm upstream from the MoO_3 and Te mixture. Before heating, the whole CVD equipment was vacuumed and purged with 200 sccm N_2 for 30 min. The reaction occurred at 1 atm pressure, with 30 sccm N_2 as the carrying gas. The furnace was heated to 600 °C at a rate of 20 °C/min and then increased to 800 °C at a rate of 5 °C/min. When the temperature of the furnace reached 800 °C, sulfur powder was heated to 120 °C and held for 10 min and then increased to 150 °C and held for 30 min. The sulfur source was further heated to 170 °C and held for 10 min before cooling down to 120 °C. The furnace was cooled down from 800 °C to room temperature rapidly by opening the furnace. The whole CVD system was home built in a fume hood to prevent possible leakage of sulfur and related volatile gases.

DOI: 10.1021/acsami.7b09807
ACS Appl. Mater. Interfaces 2017, 9, 34448−34455

3. RESULTS AND DISCUSSION

We first investigated NPL and TA processes of monolayer graphene, the energy diagrams and optical transitions of which are illustrated in Figure 2a. In our measurements, the

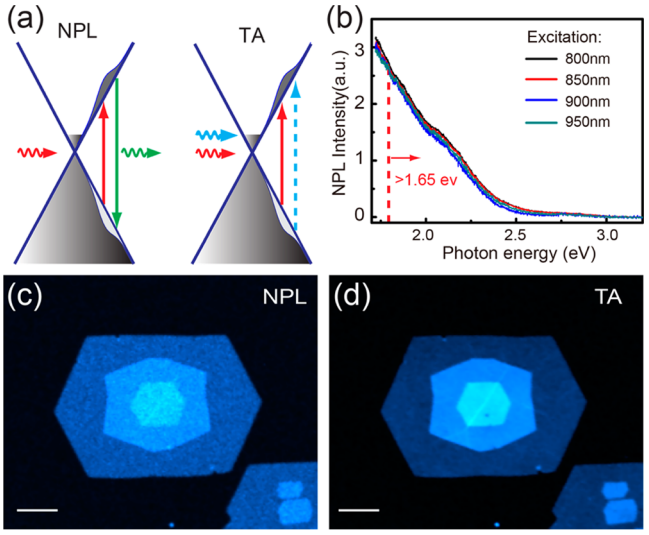

Figure 2. Characterization of NPL and TA in graphene. (a) Energy diagrams and optical transitions of NPL and TA processes, the red arrows represent photoexcitation, the green arrow represents luminescence, and the blue-dashed arrow represents TA. (b) Measured NPL spectra excited at various wavelengths. Red arrow indicates our detection band (<750 nm). A typical (c) NPL and (d) TA image of a graphene crystal. Scale bar: 10 μm.

normalized NPL spectra under different excitation wavelengths are shown in Figure 2b. As can be seen, almost identical spectral shapes were generated within our detection window (1.65−3.26 eV), which would simplify our data analysis and modeling. Representative images of NPL and TA generated from the same graphene crystal are shown in Figure 2c,d, respectively. Layer number dependences of these two types of NLO signals and TA dynamics are shown in Figure S1.

We systematically studied NPL intensities of CVD-grown monolayer graphene transferred onto different SiO_2/Si substrates. Although the gapless graphene does not luminesce under the excitation of continuous wave laser, it could easily emit broadband NPL far exceeding the photon energy of the femtosecond-excitation laser pulses. The NPL process was considered to be dominated by incoherent radiation from the hot carriers that are generated within tens of femtoseconds upon photoexcitation (Figure 2a).[30,47] The strong electron−electron and electron−phonon scatterings result in broad distribution of the hot thermalized carriers, with the emission spectra similar to that of thermal radiation.[30] The power dependence of the NPL signal showed a nonlinear relationship of $\sim P^{2.1}$ (Figure 3a), which agrees with previous studies.[47] For each sample, we applied four excitation wavelengths: 800, 900, 1000, and 1100 nm, under fixed excitation power (2 mW on sample) and detection conditions. Significant variations of NPL intensities at different SiO_2 thicknesses and excitation wavelengths were observed, and the full data set is plotted in Figure 3b; each data point represents measurements from 10 samples. Under 800 nm excitation, the mean intensity ratio of monolayer graphene on the above three substrates was about 39.5:6.8:1.0. By contrast, the ratio changed to around 1.0:2.1:1.5 under 1100 nm excitation, with representative images shown in Figure 3c. The large variation of the NPL signal indicates the importance of choosing proper substrates to achieve best sensitivity and data quality.

Because the interface between graphene and SiO_2 remained the same, we suspect that the main contribution to the signal variation was from the interference between the forward and reflected light beams from the SiO_2/Si interface, which form partial standing waves in the focal region. The constructive or destructive interference at the graphene plane results in a drastic enhancement or decrease of excitation strength, leading to the large differences observed in luminescence intensities. A similar effect was applied to realize super-resolution fluorescence microscopy using mirror substrates with various SiO_2 thicknesses on top.[48] We, thus, constructed a theoretical model based on the above considerations. First, the focusing of light field through an objective lens could be expressed as[49]

$$E_0(v, u) = A_0 \exp(ikz) \int_0^1 \exp\left\{-\frac{iu\rho^2}{2}\right\} J_0(\rho v)\rho \, d\rho \quad (1)$$

where $v = kr \sin \alpha$ and $u = 4kz \sin^2(\alpha/2)$; $k = 2\pi/\lambda$ is the wave vector; J_0 is the zeroth-order Bessel functions; α is the aperture angle of the objective; r and z are the radial and axial coordinates at the image plane, respectively, and ρ represents the reduced coordinate at the pupil plane.[49] Then, the reflected field from the SiO_2/Si interface was included to interfere with the incoming beam and resulted in the intensity profile of the excitation beam.[48]

$$E(v, u)_{exc} = E_0(v, u) + \gamma \exp(i2knd) E_0(v, -u) \quad (2)$$

where d and n are the thickness and index of refraction of SiO_2, respectively. γ is the reflection coefficient of the electric field at the SiO_2/Si interface, determined by Fresnel equations under the approximation of normal incidence, because the wave fronts become plane waves at the waist of the Gaussian beams. The dispersion of both SiO_2 and Si was considered to calculate the wavelength-dependent γ,[37] as shown in Figure S2. In addition, the calculated electric field in eq 2 could be readily converted to excitation intensity, I_{exc}. Because of their nonlinearity, emission intensities of NLO processes obey nonlinear power laws, which could be determined experimentally.

$$I_{emi} \propto \eta(\lambda) I_{exc}^{\beta} \quad (3)$$

where η represents the detection efficiency which depends on the excitation wavelength and β is the index number. In our NPL experiment, η originates from the wavelength-dependent emission efficiency within our fixed detection window (Figure 2b). We simulated the intensity profiles of 800 and 1100 nm excitation in the $x-z$ plane, as shown in Figure 4a. For 800 nm excitation, our results indicate a constructive interference at the sample plane with 125 nm SiO_2, whereas 235 and 270 nm SiO_2 introduce destructive interferences and result in a much weaker NPL. However, when we changed the excitation wavelength to 1100 nm, the 235 nm substrate provides a more constructive interference, thus generating a higher NPL signal, which agrees well with our experimental results (Figure 3c). The detected signal could be calculated by integrating the emission intensity over the sample plane ($z = 0$). The above model could simulate NPL intensities as functions of excitation wavelength and SiO_2 thickness (Figure 4b), with a constant $\eta = 1$. This could only predict the intensity ratios between different SiO_2 thicknesses under fixed excitation wavelengths but does not provide precise

DOI: 10.1021/acsami.7b09807
ACS Appl. Mater. Interfaces 2017, 9, 34448−34455

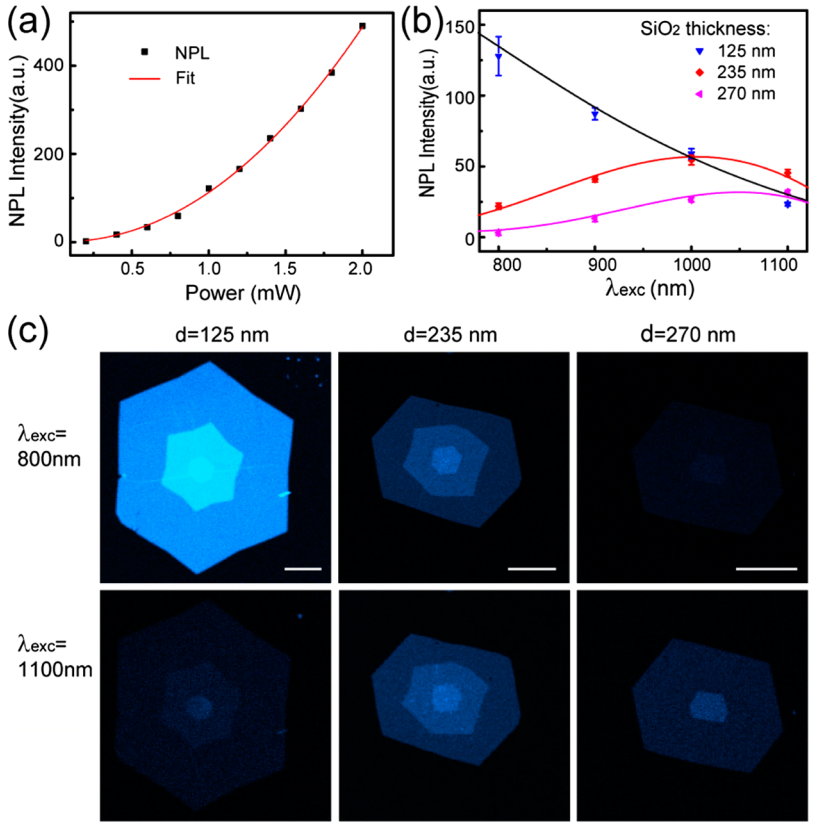

Figure 3. NPL properties in graphene with different substrates. (a) Laser power dependence of the NPL signal. (b) Measured NPL intensity at various excitation wavelengths and SiO_2 thicknesses, with simulation results plotted as solid curves. (c) Selected raw NPL images of graphene under 800 and 1100 nm excitations. Scale bar: 20 μm.

wavelength-dependent values. Accurate formulation of $\eta(\lambda)$ would require more profound physical models to simulate the NPL emission spectra and intensities under different excitation wavelengths and is beyond the scope of this study. By observing the close-to-linear behavior of the wavelength-dependent NPL signal at d = 125 nm, we applied a phenomenological linear function of $\eta(\lambda)$ as the global fitting parameter with the fitted result: $\eta(\lambda) = -0.002\lambda + 2.6$ (Figure S3). This indicates that lower excitation energies result in weaker emission intensity within our fixed detection window, which also implies lower effective emission temperature.[30] The final simulated results agree well with the whole experimental data set, as illustrated in Figure 3b.

Next, we investigated the effect of SiO_2 thickness on the TA signal. TA is a specific type of pump-probe spectroscopy that detects the differential absorbance of the probe beam induced by pump excitation. In graphene, the photoexcited hot carriers reduce the absorption of the probe beam, resulting in the increase of its intensity, and the difference signal is used to measure the strength of TA (Figure 2a). In our study, all TA data were taken under 1040 nm pump and 800 nm probe. The quadratic power dependence of TA intensity (Figure S4) reveals its third-order nonlinearity and could be described as: $S \propto [c]\cdot\sigma\cdot I_{pump}\cdot I_{probe}$.[50] The phonon-assisted relaxation of hot carriers causes a rapid decay of the TA signal within around 2 ps, as indicated in our time-resolved TA decay curves (Figure S1), which agrees with previous results.[35] Peak intensities of the TA curves were used to represent their signal strengths in this study. We measured the TA strengths of graphene on the three types of substrates, resulting in a mean intensity ratio around 2.9:2.0:1 (Figure 5a). To simulate the TA signal, our model needs to include both the pump and probe intensity profiles as results of interferences and take their product to represent the TA intensity. The simulated results are included in Figure 5a, and the calculated wavelength and SiO_2 thickness-dependent TA signal is shown in Figure 5b. Although the overall thickness dependence of TA signals appears in a similar trend as NPL, the magnitude of change is much smoother because the different pump and probe wavelengths partially smear out the variation. The intensity profiles of the product of pump and probe focal areas are calculated with different substrate thicknesses and are shown in Figure 5c.

We also briefly studied SHG intensities of monolayer MoS_2 on different thicknesses of SiO_2. Because SHG requires inversion symmetry braking, we can no longer use graphene to study SHG. To minimize the polarization dependence of SHG strength of the anisotropic MoS_2,[33] we used circular polarized light to excite the samples and detected the SHG signal without any analyzer. A typical SHG image of monolayer MoS_2 is shown in Figure 6a. The measured mean intensity ratio between different SiO_2 thicknesses is around 7.5:3.5:1, as indicated in Figure 6b. In our experiments, the excitation wavelength was fixed at 810 nm, and the SHG wavelength was 405 nm. Because SHG is a coherent process, the thin MoS_2 sheet (much thinner than the coherence length) generates similar amounts of SHG photons in both forward and backward directions with well-defined phase relations. Thus, the interference between the backward- and forward-reflected SHG photons has also been considered. The calculation of such interference is the same as in eq 2, with the electric field

DOI: 10.1021/acsami.7b09807
ACS Appl. Mater. Interfaces 2017, 9, 34448−34455

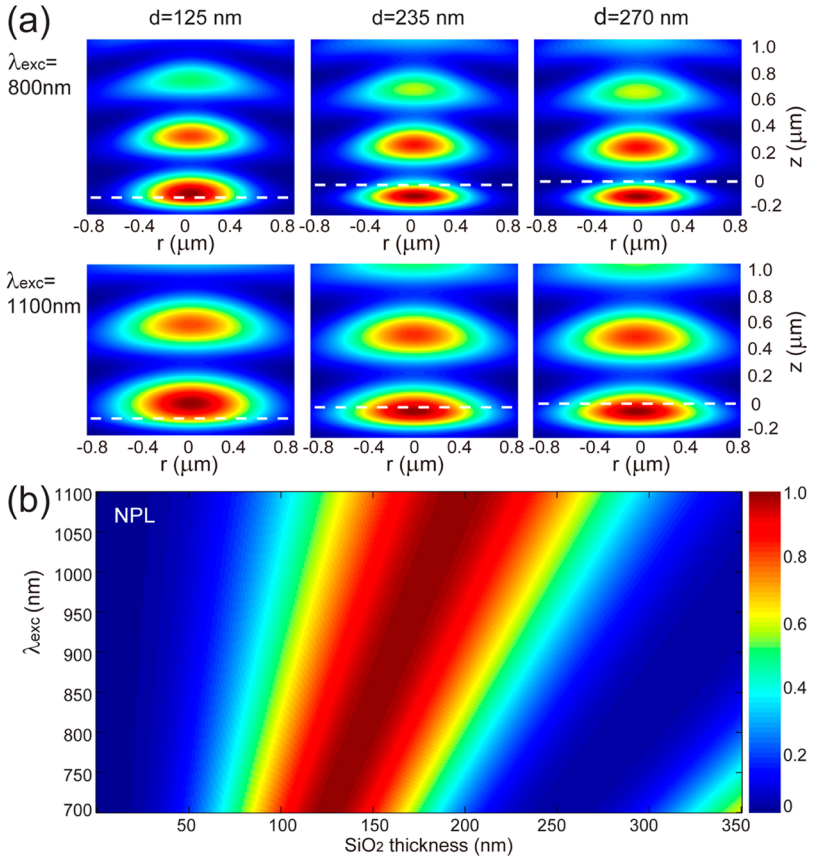

Figure 4. Simulation results for NPL. (a) Laser intensity profiles in the $r-z$ plane near laser focus for different SiO_2 thicknesses, where the sample planes are marked by the dashed lines. (b) Calculated NPL signal strength as functions of the excitation wavelength and SiO_2 thickness, assuming constant emission efficiency.

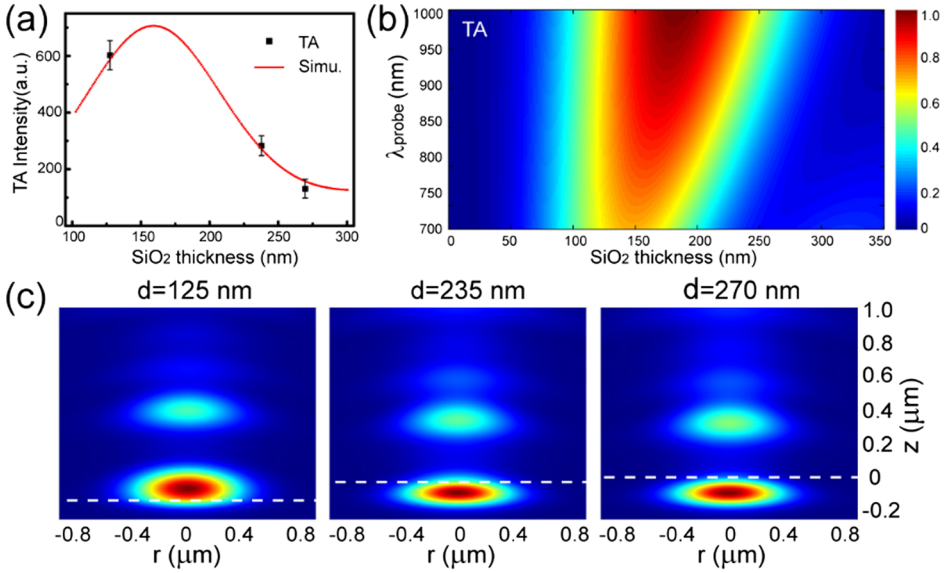

Figure 5. SiO_2 thickness-dependent TA signals. (a) Measured and simulated TA signals. (b) Calculated TA intensities as functions of probe wavelength and SiO_2 thickness. (c) Simulated intensity profiles of $I_{pump} \cdot I_{probe}$ for different SiO_2 thicknesses near laser focus. The dashed lines represent sample planes.

replaced by the SHG field and the phase and reflection coefficient adjusted according to the SHG wavelength. Taking account of the interferences of both excitation and emission beams, we could calculate the angular distribution of SHG intensities integrated over a solid angle determined by the objective numerical aperture. With the second-order nonlinearity ($\beta = 2$), our simulated results qualitatively agree with the experimental data (Figure 6b), and the calculated SHG intensity as functions of excitation wavelength and SiO_2 thickness is shown in Figure 6c. Because the excitation and

DOI: 10.1021/acsami.7b09807
ACS Appl. Mater. Interfaces 2017, 9, 34448−34455

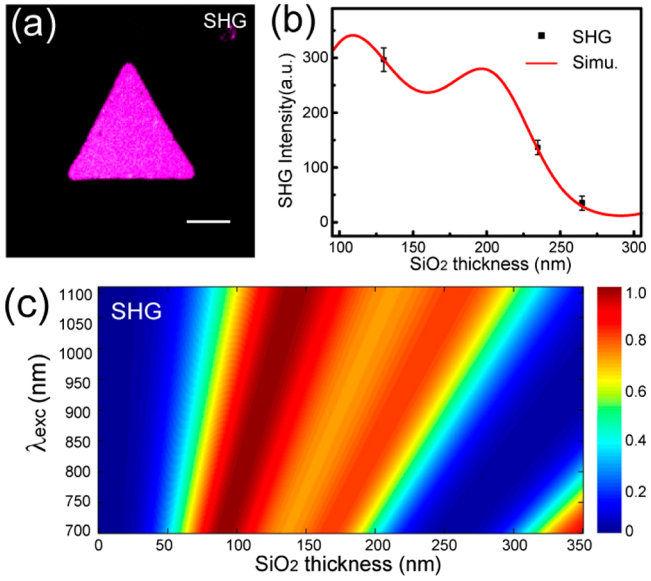

Figure 6. SHG signal of MoS_2 on different thicknesses of SiO_2 substrates. (a) Typical SHG image of monolayer MoS_2 crystal. (b) Measured and simulated SHG signals under 810 nm excitation. (c) Calculated SHG intensities as functions of excitation wavelength and SiO_2 thickness. Scale bar: 5 μm.

emission wavelengths have a fixed 2:1 ratio, the overall interference effect appears to have a broader enhancing region, particularly for SiO_2 thickness within 100−200 nm.

Notice that our simplified model has ignored the reflections at the interfaces of graphene/air and graphene/SiO_2 and multireflections between these interfaces. A more rigorous theory might involve solving the density matrix equation and considering multireflections and interferences of both excitation and emission fields. Nonetheless, we found that our calculations qualitatively agree with the experimental results. Although we did not measure other NLO processes, such as FWM, THG, and TPA, they should in principle fit one of the above three categories and thus could be treated in a similar way. Our model allows a quick estimate of how the substrate thickness and excitation wavelength would affect the NLO signal strength. For example, our approach might partly explain the large differences between $\chi^{(3)}$ measurements of graphene (using THG) on 300 nm SiO_2 under the excitation wavelengths of 789, 1550, and 1720 nm.[23,43,44] Moreover, microscope objectives with different NAs would affect the intensity profiles of laser focus; thus, additional care needs to be taken when choosing objectives. For instance, high NA objective results in a short Rayleigh range (focal depth) of the focal spot, which will deviate from our plane-wave approximation for the calculation of interference.[38] This is quite different from the linear optics of 2D materials, where the illumination light could be treated as pure plane waves.[37]

Although the contact of SiO_2 and graphene has noticeable doping effect owing to charge exchange at the interface, which shifts the graphene Fermi level,[51,52] it would not affect our results in this study. First of all, the change of the Fermi level induced by SiO_2 doping is around 0.1 V,[51] far below the photon energies used in the measurements and should not significantly alter the NLO signals. Moreover, doping only happens at the graphene/SiO_2 interface, which is expected to cause minimum differences between SiO_2 thickness greater than 100 nm.[53] Our Raman measurements of single-layer graphene on different SiO_2 thicknesses also indicate that all of the samples used in this study were p-doped (Figure S5).[51]

4. CONCLUSIONS

We have systematically studied the dependence of NLO signals of 2D materials on the thickness of SiO_2 in SiO_2/Si substrates. Although it might not affect the electrical measurements, we found that it has a great impact on the NLO intensities, mainly through the interference of the incoming and reflected excitation beams. Three major types of NLO processes were investigated, and the theoretical models were given to analyze the experimental data. In general, our results indicate that SiO_2 thickness between 100 and 200 nm would be better suited for most of the NLO measurements under near-infrared light excitation within 700−1100 nm spectral window. The efficiency of NLO signal generations not only determines the sensitivity of these measurements but also critically affects the application of NLO microscopy for studying various 2D materials. Echoing with the substrate-dependent linear optical studies, our work may pave the way to optimize the NLO research for 2D materials and make it more accessible and standard for the community.

■ ASSOCIATED CONTENT

Supporting Information

The Supporting Information is available free of charge on the ACS Publications website at DOI: 10.1021/acsami.7b09807.

Characterization of NPL and TA properties in graphene; simulated results of graphene NPL and $\eta(\lambda)$; and power dependence of TA and Raman spectra of graphene on different substrates (PDF)

■ AUTHOR INFORMATION

Corresponding Authors

*E-mail: zhengzong_sun@fudan.edu.cn (Z.S.).
*E-mail: minbiaoj@fudan.edu.cn (M.J.).

ORCID

Zhengzong Sun: 0000-0002-3710-4001
Minbiao Ji: 0000-0002-9066-4008

Author Contributions

⊥X.M. and N.X. contributed equally. M.J. and Z.S. conceived the experiment; X.M., Q.L., and W.W. took the optical measurements; and N.X. and H.L. synthesized the samples. The manuscript was written through contributions of all authors. All authors have given approval to the final version of the manuscript.

Notes

The authors declare no competing financial interest.

■ ACKNOWLEDGMENTS

We would like to thank Dr. W. T. Liu and Dr. S. W. Wu at Fudan University for helpful discussions. We acknowledge the financial supports from the National Key R&D Program of China (2016YFC0102100, 2016YFA0301000, 2016YFA0203900, and 2017YFA0207303); the National Natural Science Foundation of China (81671725); the Shanghai Rising Star Program (15QA1400500); and the Shanghai Action Plan for Scientific and Technological Innovation Program (16441909200).

DOI: 10.1021/acsami.7b09807
ACS Appl. Mater. Interfaces 2017, 9, 34448−34455

REFERENCES

(1) Beenakker, C. W. J. Colloquium: Andreev Reflection and Klein Tunneling in Graphene. *Rev. Mod. Phys.* **2008**, *80*, 1337−1354.
(2) Behnia, K. Condensed-Matter Physics: Polarized L Boosts Valleytronics. *Nat. Nanotechnol.* **2012**, *7*, 488−489.
(3) Ge, S.; Li, C.; Zhang, Z.; Zhang, C.; Zhang, Y.; Qiu, J.; Wang, Q.; Liu, J.; Jia, S.; Feng, J.; Dong, S. Dynamical Evolution of Anisotropic Response in Black Phosphorus under Ultrafast Photoexcitation. *Nano Lett.* **2015**, *15*, 4650−4656.
(4) Li, L.; Yu, Y.; Ye, G. J.; Ge, Q.; Ou, X.; Wu, H.; Feng, D.; Chen, X. H.; Zhang, Y. Black Phosphorus Field-Effect Transistors. *Nat. Nanotechnol.* **2014**, *9*, 372−377.
(5) Radisavljevic, B.; Kis, A. Mobility Engineering and A Metal−Insulator Transition in Monolayer MoS_2. *Nat. Mater.* **2013**, *12*, 815−820.
(6) Wang, H.; Yu, L.; Lee, Y.-H.; Shi, Y.; Hsu, A.; Chin, M. L.; Li, L.-J.; Dubey, M.; Kong, J.; Palacios, T. Integrated Circuits Based on Bilayer MoS_2 Transistors. *Nano Lett.* **2012**, *12*, 4674−4680.
(7) Baugher, B. W. H.; Churchill, H. O. H.; Yang, Y.; Jarillo-Herrero, P. Optoelectronic Devices Based on Electrically Tunable p−n Diodes in a Monolayer Dichalcogenide. *Nat. Nanotechnol.* **2014**, *9*, 262−267.
(8) Zhang, Y. J.; Oka, T.; Suzuki, R.; Ye, J. T.; Iwasa, Y. Electrically Switchable Chiral Light-Emitting Transistor. *Science* **2014**, *344*, 725−728.
(9) Cheng, R.; Li, D.; Zhou, H.; Wang, C.; Yin, A.; Jiang, S.; Liu, Y.; Chen, Y.; Huang, Y.; Duan, X. Electroluminescence and Photocurrent Generation from Atomically Sharp WSe_2/MoS_2 Heterojunction p−n Diodes. *Nano Lett.* **2014**, *14*, 5590−5597.
(10) Ryzhii, V.; Ryzhii, M.; Svintsov, D.; Leiman, V.; Mitin, V.; Shur, M. S.; Otsuji, T. Nonlinear Response of Infrared Photodetectors Based on van der Waals Heterostructures with Graphene Layers. *Opt. Express* **2017**, *25*, 5536−5549.
(11) Zhang, K.; Fang, X.; Wang, Y.; Wan, Y.; Song, Q.; Zhai, W.; Li, Y.; Ran, G.; Ye, Y.; Dai, L. Ultrasensitive Near-Infrared Photodetectors Based on a Graphene−MoTe2−Graphene Vertical van der Waals Heterostructure. *ACS Appl. Mater. Interfaces* **2017**, *9*, 5392−5398.
(12) Niu, X.; Li, Y.; Shu, H.; Yao, X.; Wang, J. Efficient Carrier Separation in Graphitic Zinc Oxide and Blue Phosphorus van der Waals Heterostructure. *J. Phys. Chem. C* **2017**, *121*, 3648−3653.
(13) Nair, R. R.; Blake, P.; Grigorenko, A. N.; Novoselov, K. S.; Booth, T. J.; Stauber, T.; Peres, N. M. R.; Geim, A. K. Fine Structure Constant Defines Visual Transparency of Graphene. *Science* **2008**, *320*, 1308.
(14) Splendiani, A.; Sun, L.; Zhang, Y.; Li, T.; Kim, J.; Chim, C.-Y.; Galli, G.; Wang, F. Emerging Photoluminescence in Monolayer MoS2. *Nano Lett.* **2010**, *10*, 1271−1275.
(15) Cao, T.; Wang, G.; Han, W.; Ye, H.; Zhu, C.; Shi, J.; Niu, Q.; Tan, P.; Wang, E.; Liu, B.; Feng, J. Valley-Selective Circular Dichroism of Monolayer Molybdenum Disulphide. *Nat. Commun.* **2012**, *3*, 887−892.
(16) Wang, X.; Jones, A. M.; Seyler, K. L.; Tran, V.; Jia, Y.; Zhao, H.; Wang, H.; Yang, L.; Xu, X.; Xia, F. Highly Anisotropic and Robust Excitons in Monolayer Black Phosphorus. *Nat. Nanotechnol.* **2015**, *10*, 517−521.
(17) Li, L.; Kim, J.; Jin, C.; Ye, G. J.; Qiu, D. Y.; da Jornada, F. H.; Shi, Z.; Chen, L.; Zhang, Z.; Yang, F. Direct Observation of The Layer-Dependent Electronic Structure in Phosphorene. *Nat. Nanotechnol.* **2017**, *12*, 21−25.
(18) Zhang, G.; Huang, S.; Chaves, A.; Song, C.; Özçelik, V. O.; Low, T.; Yan, H. Infrared Fingerprints of Few-Layer Black Phosphorus. *Nat. Commun.* **2017**, *8*, 14071.
(19) Zeng, H.; Liu, G.-B.; Dai, J.; Yan, Y.; Zhu, B.; He, R.; Xie, L.; Xu, S.; Chen, X.; Yao, W.; Cui, X. Optical Signature of Symmetry Variations and Spin-Valley Coupling in Atomically Thin Tungsten Dichalcogenides. *Sci. Rep.* **2013**, *3*, 1608.
(20) Kumar, N.; Najmaei, S.; Cui, Q.; Ceballos, F.; Ajayan, P. M.; Lou, J.; Zhao, H. Second Harmonic Microscopy of Monolayer MoS_2. *Phys. Rev. B: Condens. Matter Mater. Phys.* **2013**, *87*, 161403.
(21) Li, Y.; Rao, Y.; Mak, K. F.; You, Y.; Wang, S.; Dean, C. R.; Heinz, T. F. Probing Symmetry Properties of Few-Layer MoS_2 and H-BN by Optical Second-Harmonic Generation. *Nano Lett.* **2013**, *13*, 3329−3333.
(22) Dean, J. J.; van Driel, H. M. Second Harmonic Generation from Graphene and Graphitic Films. *Appl. Phys. Lett.* **2009**, *95*, 261910.
(23) Hong, S.-Y.; Dadap, J. I.; Petrone, N.; Yeh, P.-C.; Hone, J.; Osgood, R. M., Jr. Optical Third-Harmonic Generation in graphene. *Phys. Rev. X* **2013**, *3*, 021014.
(24) Hendry, E.; Hale, P. J.; Moger, J.; Savchenko, A. K.; Mikhailov, S. A. Coherent Nonlinear Optical Response of Graphene. *Phys. Rev. Lett.* **2010**, *105*, 097401.
(25) Brinkley, M. K.; Abergel, D. S. L.; Clader, B. D. Two-Photon Absorption in Gapped Bilayer Graphene with a Tunable Chemical Potential. *J. Phys.: Condens. Matter* **2016**, *28*, 365001.
(26) Wang, Y. W.; Liu, S.; Zeng, B. W.; Huang, H.; Xiao, J.; Li, J. B.; Long, M. Q.; Xiao, S.; Yu, X. F.; Gao, Y. L.; He, J. Ultraviolet Saturable Absorption and Ultrafast Carrier Dynamics in Ultrasmall Black Phosphorus Quantum Dots. *Nanoscale* **2017**, *9*, 4683−4690.
(27) Sharma, R.; Aneesh, J.; Yadav, R. K.; Sanda, S.; Barik, A. R.; Mishra, A. K.; Maji, T. K.; Karmakar, D.; Adarsh, K. V. Strong Interlayer Coupling Mediated Giant Two-Photon Absorption in MoSe2/Graphene Oxide Heterostructure: Quenching of Exciton Bands. *Phys. Rev. B* **2016**, *93*, 155433.
(28) Anand, B.; Podila, R.; Lingam, K.; Krishnan, S. R.; Sai, S. S. S.; Philip, R.; Rao, A. M. Optical Diode Action from Axially Asymmetric Nonlinearity in an All-Carbon Solid-State Device. *Nano Lett.* **2013**, *13*, 5771−5776.
(29) Sun, Z.; Hasan, T.; Torrisi, F.; Popa, D.; Privitera, G.; Wang, F.; Bonaccorso, F.; Basko, D. M.; Ferrari, A. C. Graphene Mode-Locked Ultrafast Laser. *ACS Nano* **2010**, *4*, 803−810.
(30) Lui, C. H.; Mak, K. F.; Shan, J.; Heinz, T. F. Ultrafast Photoluminescence from Graphene. *Phys. Rev. Lett.* **2010**, *105*, 127404.
(31) Li, W.; Chen, B.; Meng, C.; Fang, W.; Xiao, Y.; Li, X.; Hu, Z.; Xu, Y.; Tong, L.; Wang, H.; Liu, W.; Bao, J.; Shen, Y. R. Ultrafast All-Optical Graphene Modulator. *Nano Lett.* **2014**, *14*, 955−959.
(32) Liu, W.-T.; Wu, S. W.; Schuck, P. J.; Salmeron, M.; Shen, Y. R.; Wang, F. Nonlinear Broadband Photoluminescence of Graphene Induced by Femtosecond Laser Irradiation. *Phys. Rev. B: Condens. Matter Mater. Phys.* **2010**, *82*, 081408.
(33) Yin, X.; Ye, Z.; Chenet, D. A.; Ye, Y.; O'Brien, K.; Hone, J. C.; Zhang, X. Edge Nonlinear Optics on a MoS_2 Atomic Monolayer. *Science* **2014**, *344*, 488−490.
(34) Zhang, L.; Shen, S.; Liu, Z.; Ji, M. Label-Free, Quantitative Imaging of MoS_2-Nanosheets in Live Cells with Simultaneous Stimulated Raman Scattering and Transient Absorption Microscopy. *Adv. Biosyst.* **2017**, *1*, 1700013.
(35) Li, J.; Zhang, W.; Chung, T.-F.; Slipchenko, M. N.; Chen, Y. P.; Cheng, J.-X.; Yang, C. Highly Sensitive Transient Absorption Imaging of Graphene and Graphene Oxide in Living Cells and Circulating Blood. *Sci. Rep.* **2015**, *5*, 12394.
(36) Xu, Y.; He, R.; Lin, D.; Ji, M.; Chen, J. Laser Beam Controlled Drug Release from Ce6−Gold Nanorod Composites in Living Cells: a FLIM study. *Nanoscale* **2015**, *7*, 2433−2441.
(37) Blake, P.; Hill, E. W.; Neto, A. H. C.; Novoselov, K. S.; Jiang, D.; Yang, R.; Booth, T. J.; Geim, A. K. Making Graphene Visible. *Appl. Phys. Lett.* **2007**, *91*, 063124.
(38) Casiraghi, C.; Hartschuh, A.; Lidorikis, E.; Qian, H.; Harutyunyan, H.; Gokus, T.; Novoselov, K. S.; Ferrari, A. C. Rayleigh Imaging of Graphene and Graphene Layers. *Nano Lett.* **2007**, *7*, 2711−2717.
(39) He, J.; He, D.; Wang, Y.; Cui, Q.; Bellus, M. Z.; Chiu, H.-Y.; Zhao, H. Exceptional and Anisotropic Transport Properties of Photocarriers in Black Phosphorus. *ACS Nano* **2015**, *9*, 6436−6442.
(40) Cunningham, G.; Khan, U.; Backes, C.; Hanlon, D.; McCloskey, D.; Donegan, J. F.; Coleman, J. N. Photoconductivity of Solution-Processed MoS_2 Films. *J. Mater. Chem. C* **2013**, *1*, 6899−6904.

DOI: 10.1021/acsami.7b09807
ACS Appl. Mater. Interfaces 2017, 9, 34448−34455

(41) Kioseoglou, G.; Hanbicki, A. T.; Currie, M.; Friedman, A. L.; Gunlycke, D.; Jonker, B. T. Valley Polarization and Intervalley Scattering in Monolayer MoS_2. *Appl. Phys. Lett.* **2012**, *101*, 221907.
(42) Ochedowski, O.; Marinov, K.; Wilbs, G.; Keller, G.; Scheuschner, N.; Severin, D.; Bender, M.; Maultzsch, J.; Tegude, F. J.; Schleberger, M. Radiation Hardness of Graphene and MoS2 Field Effect Devices Against Swift Heavy Ion Irradiation. *J. Appl. Phys.* **2013**, *113*, 214306.
(43) Kumar, N.; Kumar, J.; Gerstenkorn, C.; Wang, R.; Chiu, H.-Y.; Smirl, A. L.; Zhao, H. Third Harmonic Generation in Graphene and Few-Layer Graphite Films. *Phys. Rev. B: Condens. Matter Mater. Phys.* **2013**, *87*, 121406.
(44) Säynätjoki, A.; Karvonen, L.; Riikonen, J.; Kim, W.; Mehravar, S.; Norwood, R. A.; Peyghambarian, N.; Lipsanen, H.; Kieu, K. Rapid Large-Area Multiphoton Microscopy for Characterization of Graphene. *ACS Nano* **2013**, *7*, 8441−8446.
(45) He, R.; Xu, Y.; Zhang, L.; Ma, S.; Wang, X.; Ye, D.; Ji, M. Dual-Phase Stimulated Raman Scattering Microscopy for Real-Time Two-Color Imaging. *Optica* **2017**, *4*, 44−47.
(46) Gong, Y.; Lin, J.; Wang, X.; Shi, G.; Lei, S.; Lin, Z.; Zou, X.; Ye, G.; Vajtai, R.; Yakobson, B. I.; Terrones, H.; Terrones, M.; Tay, B. K.; Lou, J.; Pantelides, S. T.; Liu, Z.; Zhou, W.; Ajayan, P. M. Vertical and In-Plane Heterostructures from WS2/MoS2 Monolayers. *Nat. Mater.* **2014**, *13*, 1135−1142.
(47) Winzer, T.; Ciesielski, R.; Handloser, M.; Comin, A.; Hartschuh, A.; Malic, E. Microscopic View on the Ultrafast Photoluminescence from Photoexcited Graphene. *Nano Lett.* **2015**, *15*, 1141−1145.
(48) Yang, X.; Xie, H.; Alonas, E.; Liu, Y.; Chen, X.; Santangelo, P. J.; Ren, Q.; Xi, P.; Jin, D. Mirror-Enhanced Super-Resolution Microscopy. *Light: Sci. Appl.* **2016**, *5*, No. e16134.
(49) Gu, M. *Advanced Optical Imaging Theory*; Springer Science & Business Media, 2000; Vol. *75*.
(50) Min, W.; Freudiger, C. W.; Lu, S.; Xie, X. S. Coherent Nonlinear Optical Imaging: beyond Fluorescence Microscopy. *Annu. Rev. Phys. Chem.* **2011**, *62*, 507−530.
(51) Shi, Y.; Dong, X.; Chen, P.; Wang, J.; Li, L.-J. Effective Doping of Single-Layer Graphene from Underlying SiO_2 Substrates. *Phys. Rev. B: Condens. Matter Mater. Phys.* **2009**, *79*, 115402.
(52) Stampfer, C.; Molitor, F.; Graf, D.; Ensslin, K.; Jungen, A.; Hierold, C.; Wirtz, L. Raman Imaging of Doping Domains in graphene on SiO2. *Appl. Phys. Lett.* **2007**, *91*, 241907.
(53) Calizo, I.; Bao, W.; Miao, F.; Lau, C. N.; Balandin, A. A. The Effect of Substrates on the Raman Spectrum of Graphene: Graphene-on-Sapphire and Graphene-on-Glass. *Appl. Phys. Lett.* **2007**, *91*, 201904.

DOI: 10.1021/acsami.7b09807
ACS Appl. Mater. Interfaces 2017, 9, 34448−34455